

Contents

Hypoplastic and elastoplastic modelling – a comparison with test Data	1
<i>Th. MARCHER, P.A VERMEER, P.-A. von WOLFFERSDORFF</i>	
1 Introduction	1
2 Experimental data	2
3 Hypoplastic calculation	3
4 Elastoplastic calculations	8
5 Comparison	13
6 Conclusions	20
7 Acknowledgements	21
References	21

Hypoplastic and elastoplastic modelling – a comparison with test Data

Th. MARCHER¹, P.A VERMEER¹, and P.-A. von WOLFFERSDORFF²

¹ Institut für Geotechnik Universität Stuttgart

² Ed. Züblin AG, Hauptverwaltung Stuttgart, Technisches Büro Tiefbau

Abstract. A large database on Hostun RF Sand containing the results of axisymmetric and plane strain tests under drained conditions is used to compare the performance of two entirely different constitutive models: an elastoplastic and a hypoplastic model. On considering input parameters and formulations one might expect completely different stress-strain behaviour. But from the present study it will appear that model performances in relation to real soil behaviour bear a great deal of similarity.

1 Introduction

After many years of research on constitutive modelling it is interesting to pose the question: 'How far did we get in this field of research?' Considering the fact that research has been making progress in both elastoplastic modelling and hypoplastic modelling we will consider models from both frameworks.

As a representative model of hypoplasticity, attention will be focussed on the 8-parameter model by von Wolffersdorff et.al.. This model was designed to model sand behaviour at all possible densities with one single set of eight input parameters. Several of these model parameters are characteristic void ratios, e.g. the minimum, the maximum and the critical one.

As an example from the school of elastoplastic modelling we will consider the 8-parameter model by Schanz et.al. both in its original version as well as in an extended 9-parameter version. This model was designed to match not only sand behaviour, but also silt and clay. In contrast to the hypoplastic model, however, a set of parameters refers to a particular soil density. Hence two different sets of model parameters are needed when considering both a loose and a dense packing of a particular soil.

The set of parameters for this so-called Hardening Soil model (HS-model) includes conventional soil properties such as the peak friction angle and the cohesive strength. Another kind of failure parameter is the peak dilatancy angle. On top of that, the HS-model requires values for soil stiffness as measured both in triaxial and oedometer tests.

On considering input parameters and formulations, both models are entirely different and one might expect completely different stress-strain behaviour. From the present study, however, it will appear that model performances bear a great deal of similarity. The main aim of this paper is not to

compare the above constitutive models, but the performance of these models in relation to real soil behaviour.

2 Experimental data

All tests used the so-called Hostun 'RF' Sand according to [13]. This kind of quartz sand was studied extensively with different testing devices. The main part of the tests were performed at Grenoble [14–16] and another part of the experiments was carried out at Stuttgart [17,18]. The motive for all these experiments was to use the results for the development and research of constitutive models and to compare laboratory-results of newly-developed testing devices with existing data.

In order to get a satisfying comparison between the complex numerical recalculations and the experimental results, it was necessary to ensure that the input data was of high quality. Moreover it was also necessary to classify narrow ranges for the initial density to ensure comparable test results. Therefore a so called 'loose' Hostun Sand with an initial void ratio range between 0,85 - 0,92 was specified and, under drained conditions, the following test results remained for a comparison:

- 3 oedometer tests with unloading - reloading loops
- 1 triaxial compression test at 100 kPa confining pressure
- 2 triaxial compression tests at 300 kPa confining pressure
- 2 biaxial tests at 100 kPa confining pressure
- 3 torsional oedometer tests

The 'dense' Hostun Sand was specified within an initial void ratio range of 0,63 - 0,68 and therefore under the drained conditions the following test results remain at our disposal:

- 2 oedometer tests with unloading - reloading loops
- 3 triaxial compression tests at 100 kPa confining pressure
- 2 triaxial compression tests at 300 kPa confining pressure
- 2 biaxial tests at 100 kPa confining pressure
- 3 torsional oedometer tests

The data from oedometer, triaxial compression and biaxial tests are supplemented by results from a torsional shear device called 'torsional oedometer'. In this new laboratory-device, developed at the Institute of Geotechnical Engineering, Stuttgart, a disc-shaped sample with a diameter of 94 mm and a height of 25 mm is first consolidated in one dimension and afterwards sheared by torsional loading. The stresses are only measured and evaluated on a ring-shaped section of the sample according to Fig. 1. This device enables the stiffness as well as strength parameters to be evaluated within one test. Other advantages are that this device enables tests to be performed on

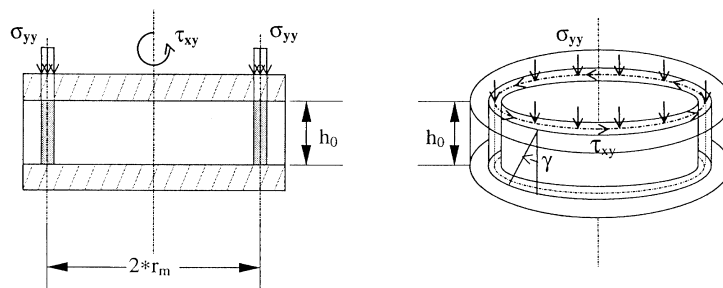


Fig. 1. Principal layout of the torsional oedometer box

undisturbed samples and that only a small amount of material is needed for one test. Such test conditions enable also the effects of stress rotations to be studied. For details of the device concept and design, the reader is referred to [18] and the recent publication [19].

3 Hypoplastic calculation

3.1 General remarks

The constitutive theory of hypoplasticity arose from the attempt to capture the behaviour of soil in as simple a mathematical structure as possible [5,6]. It is distinctive in that the most important characteristics of the mechanical behaviour of granular material are expressed in one single tensorial equation.

It differs from the elasto-plastic model in that the splitting of the deformation into an elastic and a plastic part no longer occurs and neither do the mathematical constructs such as plastic potential, yield surface, flow rule and consistency condition.

The model as used here was formulated by von Wolffersdorff [11]. The basis for it is the theoretical work on hypoplasticity by Kolymbas [5,6], Gudehus [3] and Bauer [2].

The general form for the constitutive law is:

$$\dot{\boldsymbol{\sigma}} = \mathbf{F}(\boldsymbol{\sigma}, e, \dot{\boldsymbol{\epsilon}}). \quad (1)$$

Eqn. (1) provides the stress response $\dot{\boldsymbol{\sigma}}^1$ for a given rate of deformation $\dot{\boldsymbol{\epsilon}}$ at one material point whose actual state is defined by stress $\boldsymbol{\sigma}$ and the void ratio e .

¹ An objective form of (1) is $\dot{\hat{\mathbf{T}}} = \mathbf{F}(\hat{\mathbf{T}}, e, \mathbf{D})$ [8]. $\hat{\mathbf{T}}$ is the co-rotational (JAUMANN) stress rate. It is expressed as follows $\dot{\hat{\mathbf{T}}} = \dot{\mathbf{T}} - \mathbf{W}\mathbf{T} + \mathbf{T}\mathbf{W}$ where $\dot{\mathbf{T}}$ is time derivative of CAUCHY stress \mathbf{T} . The spin tensor \mathbf{W} is the antisymmetric part of the velocity gradient $\text{grad } \mathbf{v}$, i.e. $\mathbf{W} = (\text{grad } \mathbf{v} - (\text{grad } \mathbf{v})^T)/2$, the stretching tensor \mathbf{D} is the corresponding symmetric part, i.e. $\mathbf{D} = (\text{grad } \mathbf{v} + (\text{grad } \mathbf{v})^T)/2$. The notation in this paper based on the linear theory of strains, i.e. $\dot{\boldsymbol{\epsilon}}$ is the infinitesimal strain and $\boldsymbol{\sigma}$ is the stress.

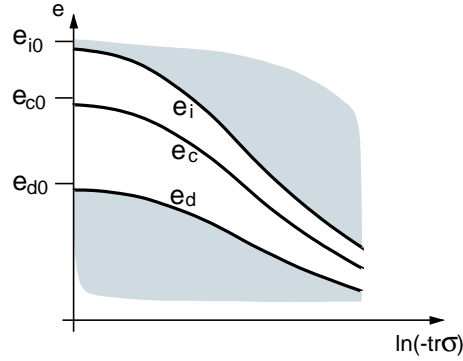


Fig. 2. The range of possible void ratios as a function of stress level. The upper limit void ratios is denoted as e_i , lower limit void ratios as e_d and the critical void ratios as e_c .

The void ratio \dot{e} relates to the rate of volumetric strain, i.e.:

$$\dot{e} = (1 + e)\text{tr} \dot{\epsilon} \quad (2)$$

In the constitutive law, the influence of the pressure level and the density on the behaviour of soil or granular materials is taken into consideration. Stiffness, shearing dilatancy or contractancy and the peak friction result from the actual condition of the soil elements and the direction of the deformation.

3.2 Hypoplastic model

The theoretical basis and the deduction of the hypoplastic relationship are described in detail in [1-3,10,11]. Here, only the two most fundamental characteristics of the material law will be explained.

The range of possible void ratios depends on the pressure (see Fig. 2). The upper limit is e_i , the lower e_d , and e_c is the void ratio at critical state. With increasing mean stress both e_i , e_d and e_c decrease in accordance with one and the same law of compression (see Eqn. (12)).

Critical conditions can occur where the granulate has a particular void ratio dependent on the pressure and the plastic flow is ideal. The critical stress σ_c fulfils the yield function according to Matsuoka/Nakai [7] (see Fig. 3). The width of the opening of this cone-shaped limiting surface is determined by the critical friction angle φ_c .

In Vermeers representation [9], it is as follows:

$$f = \frac{J_3}{J_1 J_2} + \frac{\cos^2 \varphi_c}{9 - \sin^2 \varphi_c} = 0. \quad (3)$$

with the stress invariants

$$J_1 = \text{tr} \sigma, J_2 = \frac{1}{2} (\text{tr} (\sigma^2) - J_1^2), J_3 = \det[\sigma].$$

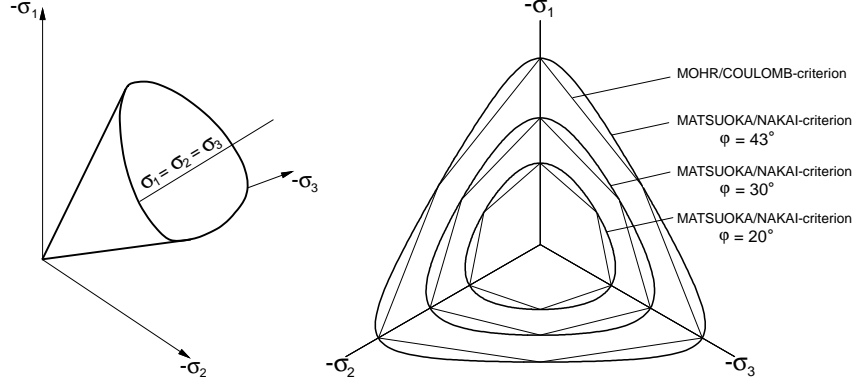


Fig. 3. The limit surface by MATSUOKA/NAKAI.

To implement the yield condition according to Matsuoka/Nakai in the hypoplastic model, the following form is more useful:

$$f = \frac{1}{2} \text{tr}(\hat{\sigma}^{*2}) - F^2 \frac{4 \sin^2 \varphi_c}{3(3 - \sin \varphi_c)^2} = 0 \quad (4)$$

with

$$F = \sqrt{\frac{1}{8} \tan^2 \psi + \frac{2 - \tan^2 \psi}{2 + \sqrt{2} \tan \psi \cos 3\vartheta}} - \frac{1}{2\sqrt{2}} \tan \psi$$

and with the invariant angle functions

$$\tan \psi = \sqrt{3} \|\hat{\sigma}^*\| \quad (5)$$

and

$$\cos 3\vartheta = -\sqrt{6} \frac{\text{tr}(\hat{\sigma}^{*3})}{[\text{tr}(\hat{\sigma}^{*2})]^{3/2}} \quad (6)$$

Fig. 4 shows the definitions of both angle functions in the principal stress space.

The hypoplastic law of material is described completely by the tensorial equation (7) together with (8), (9), (10), (11) and (12):

$$\dot{\hat{\sigma}} = f_s \frac{1}{\text{tr}(\hat{\sigma}^2)} \left\{ F^2 \dot{\hat{\epsilon}} + a^2 \text{tr}(\hat{\sigma} \dot{\hat{\epsilon}}) \hat{\sigma} + f_d a F [\hat{\sigma} + \hat{\sigma}^*] \|\dot{\hat{\epsilon}}\| \right\} \quad (7)$$

$$\text{with } \hat{\sigma} = \sigma / \text{tr } \sigma \text{ and } \hat{\sigma}^* = \hat{\sigma} - \frac{1}{3} \mathbf{1}.$$

The parameter a in (7) results from the analogous result (4) from

$$a = \frac{\sqrt{3} (3 - \sin \varphi_c)}{2\sqrt{2} \sin \varphi_c}. \quad (8)$$

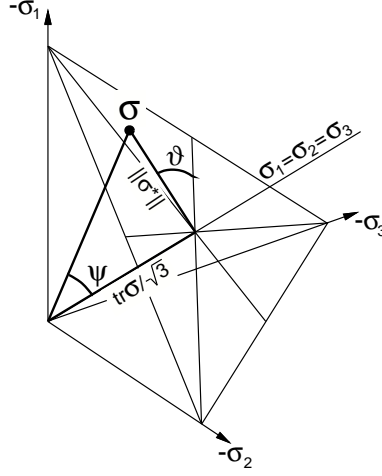


Fig. 4. The geometrical representation of the invariants $\tan \psi$ and $\cos 3\theta$ in the space of principal stresses.

F is the stress function according to Matsuoka/Nakai

$$F = \sqrt{\frac{1}{8} \tan^2 \psi + \frac{2 - \tan^2 \psi}{2 + \sqrt{2} \tan \psi \cos 3\theta}} - \frac{1}{2\sqrt{2}} \tan \psi \quad (9)$$

with $\tan \psi$ and $\cos 3\theta$ according to (5) and (6). The scalar factors

$$f_d = \left(\frac{e - e_d}{e_c - e_d} \right)^\alpha \quad (10)$$

and

$$f_s = \frac{h_s}{n} \left(\frac{1 + e_i}{e_i} \right) \left(\frac{e_i}{e} \right)^\beta \left(-\frac{\text{tr } \boldsymbol{\sigma}}{h_s} \right)^{1-n} \left[3 + a^2 - \sqrt{3}a \left(\frac{e_{i0} - e_{d0}}{e_{c0} - e_{d0}} \right)^\alpha \right]^{-1} \quad (11)$$

are functions of the pressure $\text{tr } \boldsymbol{\sigma}$ and the void ratio e . The law of compression for the pressure-dependence decline of the void ratios e_i , e_d and e_c is

$$\frac{e_i}{e_{i0}} = \frac{e_c}{e_{c0}} = \frac{e_d}{e_{d0}} = \exp \left[- \left(-\frac{\text{tr } \boldsymbol{\sigma}}{h_s} \right)^n \right]. \quad (12)$$

In the oedometer test and in the conventional triaxial tests, the axisymmetric conditions, that is $\sigma_2 = \sigma_3$ as well as $\varepsilon_2 = \varepsilon_3$ are valid. Because of this, the hypoplastic law is clearly simplified and can be expressed by the following two equations:

$$\dot{\sigma}_1 = f_s \frac{(\sigma_1 + 2\sigma_2)^2}{\sigma_1^2 + 2\sigma_2^2} \left\{ F^2 \dot{\varepsilon}_1 + a^2 \frac{(\sigma_1 \dot{\varepsilon}_1 + 2\sigma_2 \dot{\varepsilon}_2) \sigma_1}{(\sigma_1 + 2\sigma_2)^2} + \right. \quad (13)$$

$$\left. f_d a F \frac{1}{3} \frac{5\sigma_1 - 2\sigma_2}{\sigma_1 + 2\sigma_2} \sqrt{\dot{\varepsilon}_1^2 + 2\dot{\varepsilon}_2^2} \right\} \quad (14)$$

$$\dot{\sigma}_2 = f_s \frac{(\sigma_1 + 2\sigma_2)^2}{\sigma_1^2 + 2\sigma_2^2} \left\{ F^2 \dot{\varepsilon}_2 + a^2 \frac{(\sigma_1 \dot{\varepsilon}_1 + 2\sigma_2 \dot{\varepsilon}_2) \sigma_2}{(\sigma_1 + 2\sigma_2)^2} + \right. \quad (15)$$

$$\left. f_d a F \frac{1}{3} \frac{4\sigma_2 - \sigma_1}{\sigma_1 + 2\sigma_2} \sqrt{\dot{\varepsilon}_1^2 + 2\dot{\varepsilon}_2^2} \right\} \quad (16)$$

$$\text{with } F = \begin{cases} 1 & \text{for } \sigma_1 \leq \sigma_2 = \sigma_3 \\ \frac{2\sigma_1 + \sigma_2}{\sigma_1 + 2\sigma_2} & \text{for } \sigma_1 > \sigma_2 = \sigma_3 \end{cases}$$

In (14) and (17), the time derivatives of the actual stress σ_i and the logarithmic strain ε_i are $\dot{\sigma}_i$ and $\dot{\varepsilon}_i$.

3.3 Parameters of the hypoplastic model

The constitutive relationship requires 8 material constants, namely,

- h_s : the granular stiffness,
- n : the exponent of compression law,
- φ_c : the critical friction angle,
- e_{c0} : the critical void ratio for $\boldsymbol{\sigma} = \mathbf{0}$,
- e_{d0} : the void ratio at maximum density for $\boldsymbol{\sigma} = \mathbf{0}$,
- e_{i0} : the void ratio at minimum density for $\boldsymbol{\sigma} = \mathbf{0}$,
- α : the pycnotropy exponent,
- β : the pycnotropy exponent.

They are closely connected with the granular characteristics of the soil considered and are valid for a wide range of pressures and densities. That means that the laboratory tests carried out on densely packed sand as well as those carried out on loosely packed sand can be analysed with one and the same set of material parameters.

Herle [4] carried out extensive investigations to determine the parameters. He showed that the hypoplastic model remained sound even when there were variations to the input parameter. In addition, he developed simple methods to determine the 8 model parameters. As a rule simple index tests are all that are needed to be able to estimate most of the parameters sufficiently accurately. Herle provides sets of parameters for a total of 10 different non-cohesive soils, among others for Hostun sand. The material parameters listed there have also been used for the analysis of the laboratory tests here (see Table 1). Only φ_c and α have been slightly adjusted for better fitting test results.

φ_c [°]	h_s [MPa]	n	e_{c0}	e_{d0}	e_{i0}	α	β
32	1000	0,29	0,91	0,61	1,09	0,19	2,0

Table 1. Parameter of the hypoplastic model for Hostun-Sand

4 Elastoplastic calculations

4.1 Characteristics of the Hardening Soil model

The elastoplastic model used is the so called Hardening Soil model according to [12]. The main characteristics of the HS model are the hardening as observed in standard triaxial tests and the stress-dependent stiffness as observed in oedometer tests. The general three-dimensional extension dates back to [20]. Subsequently a summary of the most important assumptions and approaches are given.

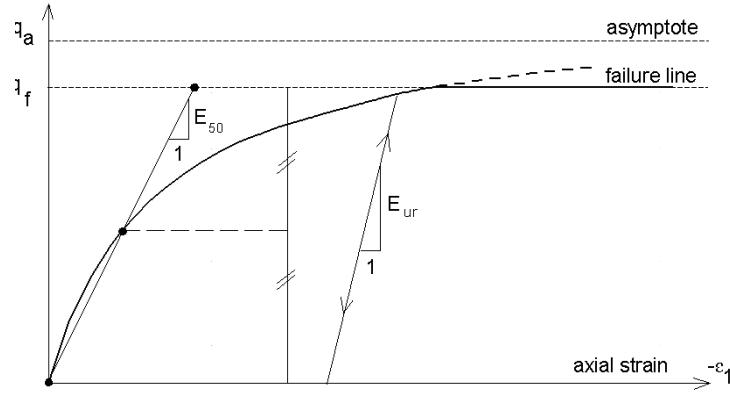


Fig. 5. Hyperbolic stress-strain relation in primary loading for a standard drained triaxial test

One basic idea of the HS-model formulation is the hyperbolic relationship between the vertical strain and the deviatoric stress in standard drained triaxial tests with constant confining pressure as illustrated in Fig. 5 (according to [21]). This relationship is described in (17):

$$\varepsilon_1 = \frac{q_a}{2E_{50}} \cdot \frac{(\sigma_1 - \sigma_3)}{q_a - (\sigma_1 - \sigma_3)} \quad (17)$$

R_f is the ratio between the ultimate deviatoric stress, q_f , and the asymptotic stress q_a according to (18). As a standard setting there is $R_f = 0,9$.

$$q_f = \frac{6 \sin \varphi_p}{3 - \sin \varphi_p} \cdot (p + c \cdot \cot \varphi_p) \quad \text{with} \quad q_a = \frac{q_f}{R_f} \quad (18)$$

Equation (18) for q_f is derived from the Mohr-Coulomb failure criterion, including a strength parameter for the cohesion c and the peak friction φ_p .

An other essential feature of the HS-model is the highly nonlinear stress-strain behaviour for primary loading and the varying stiffness for un- and reloading compared with the first loading. The E_{50} -stiffness is formulated according to [22] as a function of the actual stresses.

$$E_{50} = E_{50}^{ref} \left(\frac{\sigma_3 + c \cdot \cot \varphi_p}{\sigma_3^{ref} + c \cdot \cot \varphi_p} \right)^m \quad (19)$$

The parameter E_{50} is a stress-dependent stiffness modulus as illustrated in Fig. 5. E_{50}^{ref} is determined from a standard triaxial stress-strain-curve using the stiffness value for a mobilization of 50 % of the maximum shear strength q_f . The amount of stress dependency is given by the power m , using either experimental or empirical values. For sand, the value m is somewhere between 0,35 and 0,75.

The function 17 relates to triaxial compression conditions, but it can be extended to include general three-dimensional conditions of stress and strain. However, it is not the intention of this paper to explain models in full detail and we will not go into details of the shear-hardening formulation.

Equation (17) can be used to develop a yield function within the concept of hardening plasticity. In fact the HS-model comprises two independent yield functions and two independent yield surfaces as illustrated in Fig. 6. The most important yield function is the so-called shear yield function that relates to (17). For triaxial conditions of stress and strain the shear yield function reads

$$f^s = \bar{f} - \gamma_p \quad (20)$$

with:

$$\bar{f} = \frac{1}{E_{50}} \cdot \frac{q}{\left(1 - \frac{q}{q_a}\right)} - \frac{2q}{E_{ur}} \quad (21)$$

where E_{ur} is Young's modulus for elastic unloading and reloading and γ_p is a plastic shear strain related hardening parameter. For $f_s = 0$ and a fixed value of γ_p one obtains a shear-yield locus as indicated in Fig. 6.

In p-q-plane, the shear yield surface shown above is slightly curved, but nevertheless open in the direction of the p-axis. This implies plastic straining in deviatoric loading and fully elastic behaviour in isotropic loading. One possibility for modelling plastic straining in isotropic loading would be to modify the shear yield surface so that it intersects the p-axis. The drawback of such a single hardening model is that it gives no realistic response for overconsolidated soils. Indeed, overconsolidation would create an expansion of the

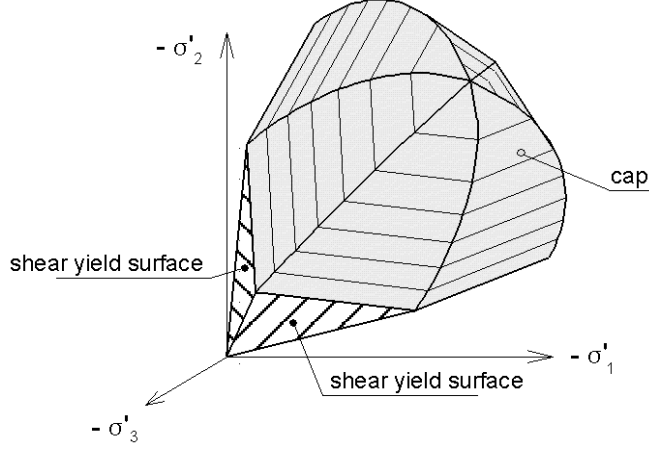


Fig. 6. Representation of total yield contour in principal stress space

entire yield surface and such models would even predict elastic behaviour in deviatoric loading. As overconsolidated soils show significant plastic straining in deviatoric loading, the idea of a single yield surface is rejected. Instead, the shear yield surface is closed by means of a yield cap, which moves independently from the shear yield surface. The shape of the cap is defined by means of the yield function

$$f^c = \bar{f}^c - p_p \quad (22)$$

with

$$\bar{f}^c = \sqrt{\frac{q^2}{\alpha^2} + p^2} - p_p \quad (23)$$

where α is an auxiliary model parameter that relates to K_0^{nc} . In fact α is chosen in such a way that $K_0^{nc} = 1 - \sin \varphi_p$. p_p is the preconsolidation pressure in isotropic loading. Between the plastic volumetric strain ε_v^p and p_p there is the relationship

$$\varepsilon_v^p = \frac{\beta}{(1+m)} \cdot \left(\frac{p_p}{p^{ref}} \right)^{1+m} \quad (24)$$

The constant β is not a direct input parameter. Instead we prefer to use a (tangent) oedometer modulus as an input parameter as explained in the next section.

The yield cap is combined with an associated flow rule to define plastic straining due to a shift of the yield cap.

For more details regarding the formulation of the HS model the reader is referred to the recent paper [23].

4.2 Parameter of the HS model

The Hardening Soil model uses a total of 8 material parameters. Three of the parameters, which are the parameters to describe the Mohr-Coloumb failure criterion, coincide with the classical Mohr-Coulomb model:

- φ_p : the peak friction angle,
- c : the cohesion,
- ψ_p : the peak dilatancy angle.

For the soil stiffness 3 basic parameters are used:

- E_{50}^{ref} : the secant stiffness,
- E_{oed}^{ref} : tangent stiffness for primary oedometer loading,
- m : the power in stiffness law.

This set of parameters are completed by the following parameters for un-reloading:

- E_{ur}^{ref} : un/reloading stiffness,
- ν_{ur} : the Poissons ratio for un/reloading.

The model presented here is developed for a geomaterial at a single initial density. This means that it does not describe the density-dependency of the strength and stiffness-parameters. For the back-calculation of the mentioned tests with the HS model one needs to define two sets of parameters, one for the calculations of the loosely packed Hostun Sand and one other for the densely packed Hostun Sand.

The HS model was calibrated by calculating triaxial compression tests and oedometer tests. The set of parameters for the 'loose' Hostun Sand is given in Table 2.

φ_p [°]	c [kPa]	ψ_p [°]	E_{50}^{ref} [kPa]	E_{oed}^{ref} [kPa]	m	E_{ur}^{ref} [kPa]	ν_{ur}
34	0	0	12000	16000	0,75	60000	0,25

Table 2. Parameter of the elastoplastic model for 'loose' Hostun Sand

Considering the experimental data for the densely packed Hostun Sand one can see that after reaching the peak strength strain-softening occurs. The following gives an extension of the general formulation of the HS model in order to describe the softening process in sand. Only thereafter will the second set of parameters be presented.

4.3 Approach for softening

The softening rule used is based on experimental results carried out at the Institute for Geotechnical Engineering, Stuttgart [24]. Drained triaxial tests were carried out on a Rhine River Sand to determine the shearing resistance of the sand. The tests were performed with different confining pressures and for varying initial void ratios. As a result, a relationship between the friction angle and the void ratio can be observed using the linear relation given in Fig. 7.

Using this observation, one can apply a basic approach for the friction softening rate according to (25) where a superimposed dot is used to denote time rates:

$$\dot{\varphi} = h_{\varphi} \cdot \dot{e} \quad (25)$$

This is a linear softening rule between the degradation of the friction angle and the rate of the void ratio. The void ratio is related to the volumetric strain according to (2) in rate form. The inverse relation is described in (26):

$$\dot{\varepsilon}_v = \frac{\dot{e}}{1 + e} \quad (26)$$

Applying this equation, the degradation of the actual friction can be controlled by the volumetric strain rate instead of the void ratio rate. In order to avoid the actual void ratio as a state parameter, this parameter is replaced in a first approach by the initial void ratio as indicated in (27):

$$\dot{\varepsilon}_v = \frac{\dot{e}}{1 + e_0} \quad (27)$$

(28) expresses the softening rule applied in the following back-calculations of experiments with densely packed Hostun Sand and implies a linear relationship between the dilation (using the volumetric strain) and the friction softening, which can be formulated in rate form as:

$$\dot{\varphi} = h_{\varphi} \cdot (1 + e_0) \cdot \dot{\varepsilon}_v \quad (28)$$

Due to the fact that the calculations are only related to one material point, the behaviour of the material is modelled in a homogeneous way. Therefore inhomogeneous deformations, as shear banding and bifurcation, are not included.

The sets of parameters for the densely packed Hostun Sand, as shown in Table 3, is extended by the softening parameter h_{φ} .

Using the two set of parameters out of Tables 2 and 3 all experiments can be recalculated. A comparison of the experimental and the two different numerical results will be presented in the next chapter.

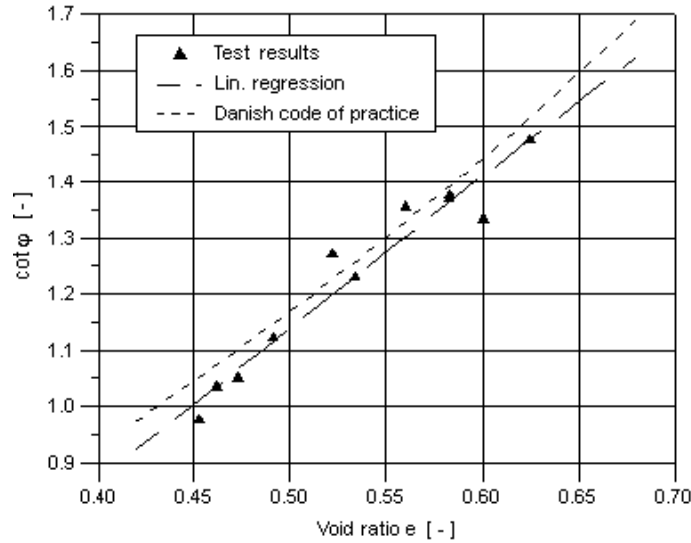


Fig. 7. Relation between friction angle φ and void ratio e

φ_p [°]	c [kPa]	ψ_p [°]	E_{50}^{ref} [kPa]	E_{oed}^{ref} [kPa]	m	E_{ur}^{ref} [kPa]	ν_{ur}	h_φ
44	0	14	30000	30000	0,55	90000	0,25	0,35

Table 3. Parameter of the elastoplastic model for 'dense' Hostun Sand

5 Comparison

A large database containing the results of tests under drained conditions is used to calibrate and verify two different constitutive models enabling a detailed comparison to be made between experimental and numerical results.

In a first step, the results of triaxial compression and oedometer tests were used to calibrate the models for the 'loose' Hostun Sand as well as for the 'dense' Hostun Sand. Then the models are applied to stress-strain conditions as encountered in biaxial tests and simple shear tests. Unfortunately simple shear tests have not been performed on Hostun Sand, but we have data of 'near' simple shear tests (torsional oedometer tests).

5.1 Comparison of results with the 'loose' Hostun Sand

Oedometer tests: For calibrating the models, data from three oedometer tests has been used including unloading-reloading loops as presented in Fig. 8. The elastoplastic model includes three un- and reloading loops at 50, 100 and 200 kPa axial load. The hypoplastic calculation includes one unloading loop at the maximum load only. In contrast to the elastoplastic type

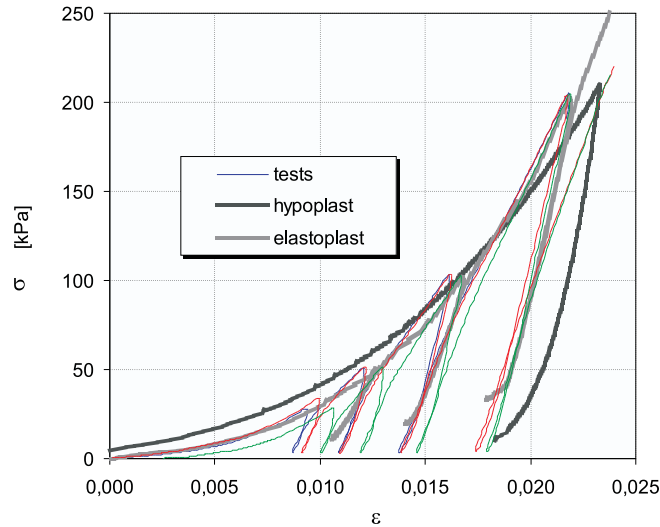


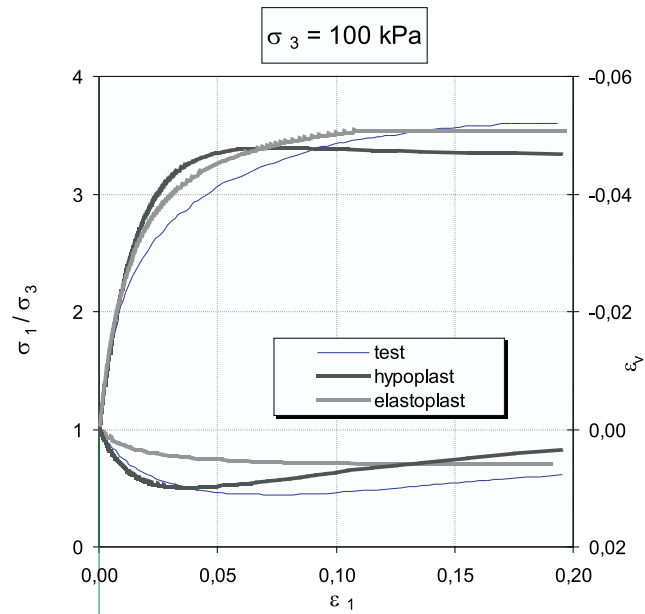
Fig. 8. Oedometer test – comparison between the numerical and experimental results on 'loose' Hostun Sand

of model, the hypoplastic model (according to [11]) cannot consistently distinguish between loading and unloading. By extending the model with the so-called 'intergranular strain' this shortcoming can be solved [25].

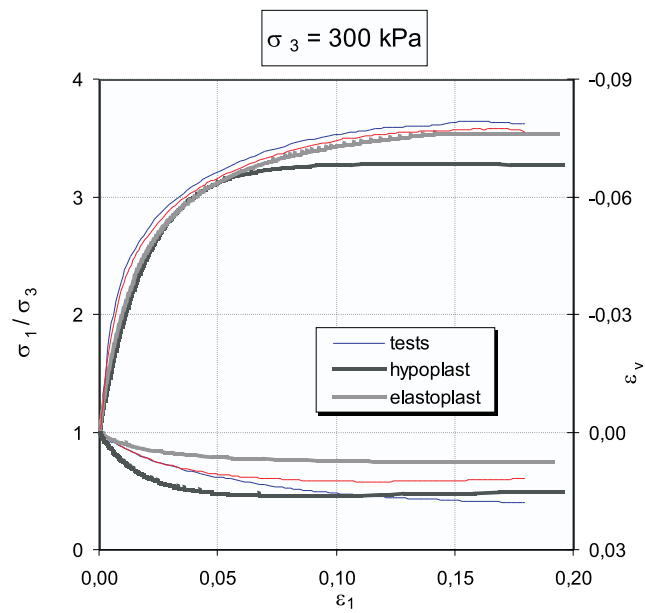
Drained triaxial tests: Figs. 9a and 9b contain two different sets of curves. One for the stress ratio as a function of axial strain and one set of curves for the volumetric strains as a function of axial strain. Fig. 9a shows data for a constant confining stress of 100 kPa whereas a confining stress of 300 kPa is considered in Fig. 9b. Unfortunately only one experiment has been performed for the lower confining stress with $\sigma_3 = 100$ kPa and this test has produced relatively large strains, at least when comparison with the data for confining stress $\sigma_3 = 300$ kPa. Nevertheless this data has been used for calibrating the input parameters of the elastoplastic model.

Biaxial tests: Fig. 10a illustrates biaxial tests with 100 kPa confining pressure. Compared to triaxial tests with the same confining pressure, biaxial tests tend to give a stiff response as also observed in Fig. 10a. Recalculating this plane-strain-problem with the two different constitutive models one can see that the stiffnesses at the beginning fit well and the maximum strength is within the range of the experimental data. Both models perform reasonably well by yielding a relatively stiff response. The hypoplastic calculation slightly overpredicts the volumetric strain.

Torsional oedometer tests: Fig. 10b presents the results for the torsional oedometer. Within this diagram, the stress ratio σ_{xy}/σ_{yy} is plotted on the left vertical axis and shear strain is on the horizontal axis. On the right axis the volumetric strain is indicated. Both models use simple shearing



a) Triaxial compression test with confining stress $\sigma_3 = 100$ kPa



b) Triaxial compression test with confining stress $\sigma_3 = 300$ kPa

Fig. 9. Triaxial compression test – comparison between the numerical and experimental results on 'loose' Hostun Sand

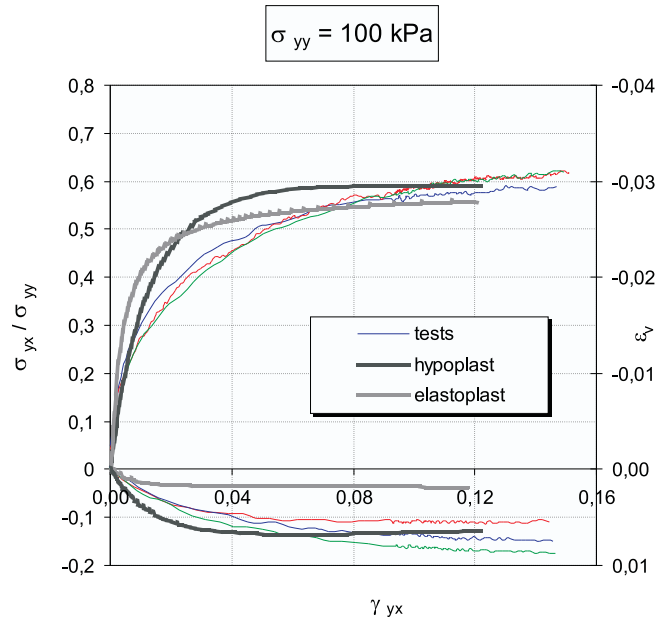
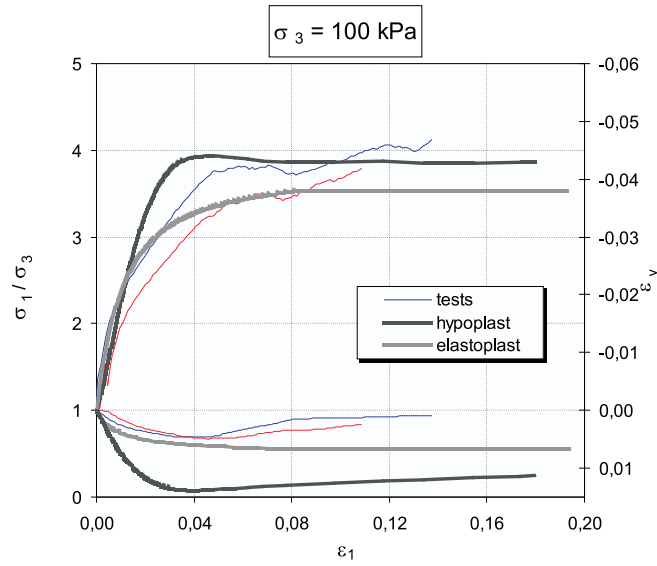


Fig. 10. Biaxial compression test and torsional oedometer test – comparison between the numerical and experimental results on 'loose' Hostun Sand

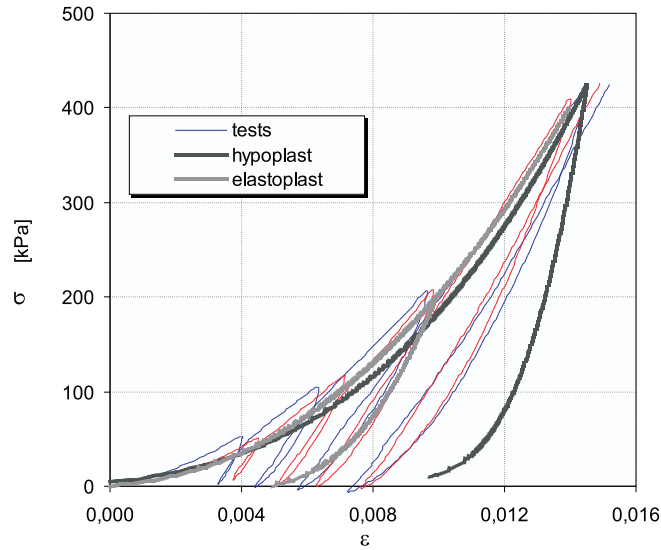


Fig. 11. Oedometer test – comparison between the numerical and experimental results on 'dense' Hostun Sand

for the recalculation of the test-data. A comparison shows that both calculations overpredict the real soil stiffness significantly, but the hypoplastic model performs better, both on the stiffness and the volumetric strain.

5.2 Comparison of results with the 'dense' Hostun Sand

Oedometer tests: When the numerical calculations are compared to the oedometer test performed using the 'dense' Hostun Sand according to Fig. 11, there is a high degree of conformity. For the elastoplastic model, one unloading loop at $\sigma_1 = 200$ kPa was performed and with the hypoplastic model one unloading loop at the maximum vertical load was calculated. As usual, data from tests on dense sand tend to show relatively little difference between first loading and unloading-reloading. In general recoverable strains tend to be of the same order of magnitude as the irrecoverable strains. In elastoplasticity this is well modelled, but the hypoplastic formulation is slightly off.

Drained triaxial tests: Figs. 12a and 12b illustrate data for confining pressures of 100 kPa and 300 kPa respectively. The models match the beginning of loading reasonably well, but deviations can be observed at and beyond peak strength. The present elastoplastic model suffers from the shortcoming that it does not include stress level dependency of the shear strength, so that the peak stress at confining pressure $\sigma_3 = 300$ kPa is significantly overestimated. On the other hand, the present hypoplastic model overestimates the amount of softening directly beyond peak.

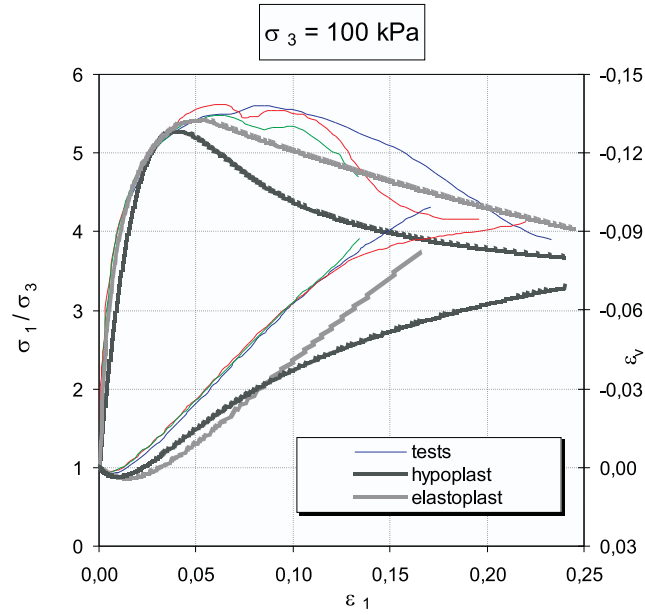
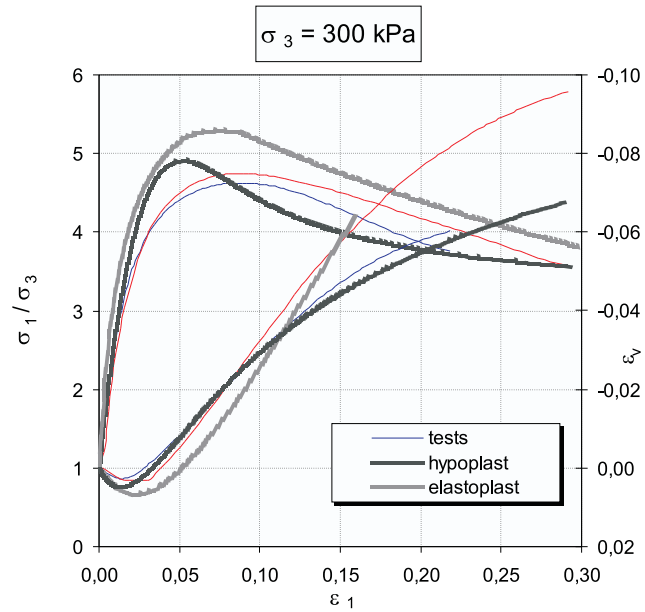
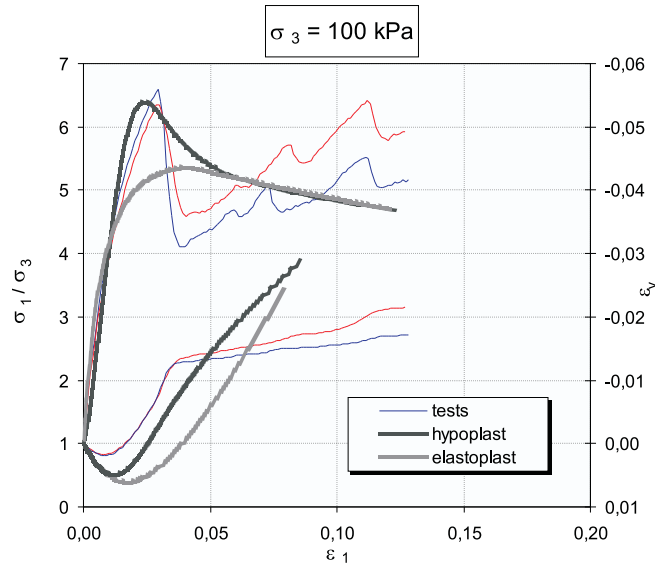
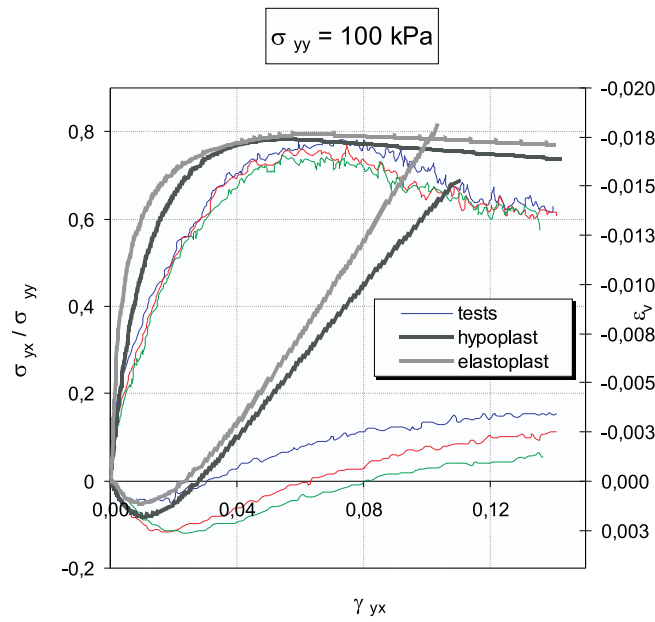
a) Triaxial compression test with confining stress $\sigma_3 = 100$ kPab) Triaxial compression test with confining stress $\sigma_3 = 300$ kPa

Fig. 12. Triaxial compression test – comparison between the numerical and experimental results on 'dense' Hostun Sand



a) Biaxial compression test with confining stress $\sigma_3 = 100$ kPa



a) Torsional oedometer test with confining stress $\sigma_{yy} = 100$ kPa

Fig. 13. Biaxial compression test and torsional oedometer test – comparison between the numerical and experimental results on 'dense' Hostun Sand

Biaxial tests: For the beginning of loading both models (according to Fig. 13a) do extremely well on the stiffness, but both of them overpredict the initial compaction of the sample. Remarkable differences occur at peak. As the present elastoplastic model involves the Mohr-Coulomb failure criterion, it underpredicts the shear strength of a sand in the biaxial mode of planar deformation to a significant extent. For a proper prediction of biaxial peak strength, one needs curved convex yield loci in the deviatoric plane of principal stress space as illustrated for the hypoplastic model in Fig. 3. As the hypoplastic model involves such a yield locus it performs much better on the biaxial strength.

Torsional oedometer tests: Finally, Fig. 13b presents the results for the torsional oedometer. A comparison shows that both calculations overpredict the soil stiffness, but the maximum strength is well predicted. Both the softening and the associated volumetric strains are poorly predicted. On the other hand, we have some doubts about the experimental data. The relatively soft response for the very beginning of loading is expected, as it has already been experienced in simple shear tests in clays, but we question the relatively low shear strength. Considering a nearly planar deformation below the measuring ring as indicated in Fig. 1, one would expect to measure high strengths just as for a biaxial test. A possible explanation would be that the bifurcation-sensitive dense sand experienced significant shear banding near and beyond peak.

6 Conclusions

On comparing a hypoplastic model with a elastoplastic model, it is immediately clear that they are formulated within entirely different frameworks of constitutive modelling. From a theoretical point of view they are thus completely different. On making a practical comparison by considering the performance of two such models, we find no basic differences at all. In fact the models we considered performed equally well for the stress and strain conditions observed. No doubt differences occur when focussing on a particular type of test, but globally speaking they performed equally well on the test data considered.

A clear operational difference between the models concern the input parameters. The hypoplastic model implies typical sand data such as void ratios. As a result one set of data suffices for all densities of a particular sand. This is an advantage when considering sands, but a disadvantage when considering other soil types, i.e. silts and clays.

Finally we have to consider the question: 'How far did we get in this field of constitutive modelling?'. Considering the data as used and produced in this paper, one would be able to give a very positive reply as our models performed reasonably well. On the other hand, it should be realised that we considered relatively simple stress paths for our comparisons. On including

undrained triaxial tests, the models may still perform quite well, but this is possibly not true for triaxial extension tests. Indeed, most researchers have developed their models with special view to triaxial compression rather than triaxial extension. For Hostun Sand, we are not even aware of data from extension tests. Similarly we did not consider data from true-triaxial testing and hollow cylinder tests. In fact, consideration of sand data is needed and this might show that we still need a good deal of research in constitutive modelling.

7 Acknowledgements

The authors thank Dr. Ivo Herle from the Institute of Theoretical and Applied Mechanics of the Czech Academy of Sciences and Dr. Paul Bonnier from PLAXIS B.V. for their support in the numerical calculation of the element tests. Thanks also to Prof. Kolymbas for suggesting us to write this article and for his valuable tips.

References

1. Bauer, E.: Zum mechanischen Verhalten granularer Stoffe unter vorwiegend ödometrischer Beanspruchung. Veröffentlichungen des Institutes für Bodenmechanik und Felsmechanik der Universität Karlsruhe, Heft **130**, 1992
2. Bauer, E.: Calibration of a comprehensive constitutive equation. Soils and Foundations, Jap. Soc. Soil Mech., **36**(1), 13-25, 1996
3. Gudehus, G.: A comprehensive constitutive equation for granular materials. Soils and Foundations, Jap. Soc. Soil Mech., **36**(1), 1-12, 1996
4. Herle, I.: Hypoplastizität und Granulometrie einfacher Korngerüste. Dissertation. Veröffentlichungen des Institutes für Bodenmechanik und Felsmechanik der Universität Karlsruhe, Heft **142**, 1997
5. Kolymbas, D.: Eine konstitutive Theorie für Böden und anderen körnige Stoffe. Habilitation. Veröffentlichungen des Institutes für Bodenmechanik und Felsmechanik der Universität Karlsruhe, Heft **109**, 1988
6. Kolymbas, D.: An outline of hypoplasticity. Archive of Applied Mechanics, **61**, 143-151, 1991
7. Matsuoka, H., Nakai, T.: Stress-strain relationship of soil based on the 'SMP'. Constitutive Equations of Soils. Proc. of Specialty Session 9, IX Int. Conf. Soil Mech. Found. Eng. Tokyo. 153-162, 1977
8. Truesdell, C., Noll, W.: The non-linear field theories of mechanics. Handbuch der Physik III/c, Springer-Verlag, 1965
9. Vermeer, P.A.: A five-constant model unifying well-established concepts. Results of the International Workshop on Constitutive Relations for Soils – Grenoble 1982. 175-198, Balkema 1982
10. Wu, W.: Hypoplastizität als mathematisches Modell zum mechanischen Verhalten granularer Stoffe. Dissertation. Veröffentlichungen des Institutes für Bodenmechanik und Felsmechanik der Universität Karlsruhe, Heft **129**, 1992

11. von Wolffersdorff, P.-A.: A hypoplastic relation for granular materials with a predefined limite state surface. *Mechanics of cohesive-frictional materials*, Vol. **1**, 251-271, 1996
12. Schanz, T.: Zur Modellierung des Mechanischen Verhaltens von Reibungsmaterialien. Habilitation, Stuttgart Universität, 1998
13. Flavigny, E., Desrues, J., Palayer, B.: Le sable d'Hostun RF. *Rev. Franc. Geotechn.*, **53**, 67-70, 1990
14. Desrues, J.: La localisation de la déformation dans les matériaux granulaires. Thèse de Docteur és Sciences, Institut de Mécanique de Grenoble, 1984
15. Hammad, W.I.: Modélisation non linéaire et étude expérimentale des bandes de cisaillement dans les sable. DSc thesis, Institut de Mécanique de Grenoble, 1991
16. Mokni, M.: Relations entre déformations en masse et déformations localisées dans les matériaux granulaires. DSc thesis, Institut de Mécanique de Grenoble, 1992
17. Schanz, T., Desrues, J., Vermeer, P.A.: Comparison of sand data on different plane strain devices. *Proceedings IS-Nagoya 97 International Symposium on Deformation and Progressive Failure in Geomechanics*, 289- 294, 1997
18. Schanz, T., Vermeer, P.A.: Das Torsionsödometer. *Institutsbericht 7* des Institutes für Geotechnik der Universität Stuttgart, 1997
19. Beutinger, P., Lindner, A., Vermeer, P.: Untersuchung von bindigen Böden im Torsionsödometer. DFG Forschungsbericht, *Institutsbericht des Institutes für Geotechnik der Universität Stuttgart*, Heft Nr. 10, 1999
20. Vermeer, P.A., Brinkgreve, R.B.J.: Plaxis; Finite element code for soil and rock analyses. Version 6, Balkema, Rotterdam, 1995
21. Kondner, R.L., Zelasko, J.S.: A hyperbolic stress strain formulation for sands. *Proc. 2nd Pan. Am. Int. Conf. Soil Mech. Found. Engrg.*, Brazil, Vol. **1**, 289-394, 1963
22. Ohde, J.: *Grundbaumechanik*. Bd. III, 27. Aufl., Hütte, 1951
23. Schanz, T., Vermeer, P.A., Bonnier, P.G.: The hardening Soil Model – Formulation and Verification. *Plaxis-Symposium: Beyond 2000 in Computational Geotechnics*, Amsterdam, 281-296, 1999
24. Vogt, C., Vermeer, P.A.: Analyses and large scale testing of plate anchors. *Proceedings of the NUMOG VII*, 1999
25. Niemunis, A., Herle, I.: Hypoplastic model for cohesionless soils with elastic strain range. *Mechanics of cohesive-frictional materials*, Vol. **2**, 279-299, 1997